

# The Maintenance of Coherent Vortex Topology by Lagrangian Chaos in Drift-Rossby Wave Turbulence

Norman M. Cao\*

*Institute for Fusion Studies, The University of Texas at Austin,  
1 University Station, Austin, Texas 78712, USA*

Di Qi†

*Department of Mathematics, Purdue University, 150 North University Street, West Lafayette, Indiana 47907, USA*  
(Dated: February 21, 2024)

This work introduces the “potential vorticity (PV) bucket brigade”, a conceptual mechanism for explaining the resilience of coherent vortex structures in drift-Rossby wave turbulence, critical for understanding turbulent transport in magnetically confined fusion plasmas and geophysical flows. Drawing parallels with the PV staircase, we show how spatially inhomogeneous patterns of mixing can reinforce, rather than destroy non-zonal structures in the flow. We accomplish this through an exact stochastic Lagrangian representation of vorticity transport, together with a wave eigenmode near-integrability property which elucidates the relationship between coherent flow topology and fluid relabeling symmetries. For concreteness, we demonstrate these ideas in a transitional regime of gradient-driven drift wave turbulence modeled by the flux-balanced Hasegawa-Wakatani equations. However, the tools we develop here are model-agnostic and have potential relevance to fluid and plasma systems well beyond the model studied here.

Despite the conception of turbulence as a mixing phenomenon, large-scale coherent structures such as jets, vortices, and waves are found to coexist with turbulence throughout geophysics, plasma physics, and beyond. Prominent examples include Jupiter’s alternating zonal bands and the coherent vortices within them [1–3], as well as Earth’s jet streams and persistent weather patterns that arise from long-lived meanders known as atmospheric blocking [4, 5]. In magnetically confined fusion plasmas, important examples include the sheared  $E \times B$  flows that form in high-confinement-mode (H-mode) plasmas [6], and zonally banded patterns of turbulence resembling “ $E \times B$  staircases” observed in simulations and experiments [7–10].

Due to the similarity in form between the magnetic and Coriolis force, strongly magnetized plasmas and strongly rotating geophysical flows exhibit strikingly analogous behaviors. A key similarity is the conservation of potential vorticity (PV) in idealized models, a scalar material invariant linked to fluid element relabeling symmetries [11–13]. Another key link is the presence of drift-Rossby waves, a class of unidirectionally propagating waves supported by fluid drifts in plasma contexts or gradients of the Coriolis parameter in geophysical contexts.

Understanding the dynamics of zonal jet flows and drift-Rossby waves in turbulent systems is crucial to unraveling the mechanisms of anomalous transport of heat and particles in magnetically confined fusion plasmas [14], characterizing energy and momentum budgets in planetary climate systems [15, 16], and enhancing the predictability of extreme weather events [17, 18]. A ma-

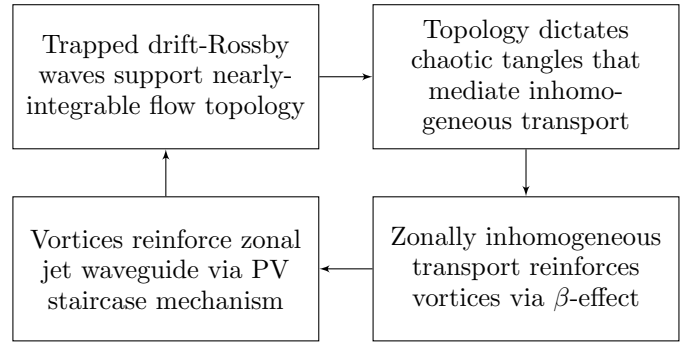


FIG. 1. Flowchart illustrating key elements of the potential vorticity bucket brigade. The two boxes on the right describe the mechanism itself, while the two on the left describe its origins.

major obstacle in this endeavour is the breaking of the statistical symmetries of turbulence by the large-scale structures. An important example of this is given by the PV staircase, used to understand the resilience of zonal jets in planetary atmospheres and magnetized plasmas [19, 20]. In the staircase paradigm, zonal flows imprint onto the statistics of the turbulence, creating a spatially inhomogeneous patterning of mixing which in turn reinforces the existing zonal flow structure. Spatial inhomogeneity precludes usage of the Wiener-Khinchin formula, so characterizations of turbulence in terms of Fourier power spectra cannot give a complete description of the two-point statistics of the velocity or other quantities.

In this work, we propose the concept of the “potential vorticity bucket brigade” as a way to understand the self-consistent transport effected by coherent vortices in 2d and quasi-2d drift-Rossby wave turbulence in the presence of zonal flows. In analogy with the PV staircase, we

\* norman.cao@austin.utexas.edu; <https://maplenormandy.github.io/>

† qidi@purdue.edu

argue that spatially inhomogeneous patterns of mixing due to the presence of coherent vortices leads to the reinforcement, rather than the destruction, of the vortices. We demonstrate how the vortex patterning can be understood through topological features of the Lagrangian flows arising from drift-Rossby eigenmodes in a zonal jet waveguide. The key ideas underlying the mechanism are illustrated in Fig. 1.

*Governing Equations.*—We study 2-dimensional plasma flows, with unit vectors  $\hat{\mathbf{x}}$  pointing radially outward and  $\hat{\mathbf{y}}$  pointing zonally in the electron diamagnetic drift direction. The geophysical equivalents are that  $\hat{\mathbf{x}}$  points northwards and  $\hat{\mathbf{y}}$  points westwards. The background magnetic field points out of the plane in the direction  $\hat{\mathbf{x}} \wedge \hat{\mathbf{y}}$ . Rossby waves and electron-branch drift waves propagate in the ‘retrograde’ direction  $\hat{\mathbf{y}}$  relative to the fluid medium. ‘Co-rotating’ vortices have an out-of-plane sense of rotation aligned with the magnetic field, and correspond to cyclones.

For concreteness, we develop the bucket brigade mechanism in the Dimits shift regime of flux-balanced Hasegawa-Wakatani (BHW) turbulence using simulation data from a previous study [21]. The Dimits shift is a transitionally turbulent regime of gradient-driven resistive drift wave turbulence where gradients are large enough to sustain a primary linear instability but not large enough to develop a uniformly turbulent state [22]. This regime is suspected to be relevant to transport in magnetically confined fusion plasmas due to rapid increase of turbulent fluxes above marginality [23]. The equations, given in the supplementary material, generalize the Charney-Hasegawa-Mima (CHM) equations [24] with a non-adiabatic electron response [25]. Length and time are normalized to the ion sound gyroradius  $\rho_s = 1$  and ion cyclotron frequency  $\omega_{ci} = 1$ , equivalent to the Rossby deformation radius and Coriolis parameter respectively.

In the absence of viscosity, the BHW equations conserve a material scalar invariant  $q + \kappa x$  called the potential vorticity (PV), related to the ion gyrocenter density [20, 26, 27]. Due to the ‘flux-balanced’ zonal density response, the BHW equations converge to the modified CHM equations in the adiabatic limit and tend to have stronger zonal flows than the modified Hasegawa-Wakatani equations [28–31]. However, the driving density gradients are still allowed to relax. This tends to create a much stronger Dimits shift, which will allow for a fairly complete description of the bucket brigade mechanism. However, the tools developed here are model-agnostic and can be easily applied to other systems.

To link Eulerian and Lagrangian representations of the flow solution, we make use of the Feynman-Kac formula, which can be thought of as a stochastic generalization of the method of characteristics. Fix a doubly periodic domain  $D = [-L_x/2, L_x/2] \times [-L_y/2, L_y/2]$ , and consider the following advection-diffusion problem for a

scalar quantity  $\chi(\mathbf{x}, t)$ ,

$$\tilde{D}_t \chi := [\partial_t + \mathbf{u}(\mathbf{x}, t) \cdot \nabla - \mu \nabla^2] \chi(\mathbf{x}, t) = f(\mathbf{x}, t); \quad (1)$$

given  $\chi(\mathbf{x}, 0)$ .

For active scalar problems, the velocity  $\mathbf{u} = (u, v)$  and forcing  $f$  can depend on  $\chi$  and other dynamical fields. Following [32], (1) is treated as a constraint that must be satisfied for independent functions  $\chi, \mathbf{u}, f$ .

Next, fix a measurement time  $T > 0$ .  $\tilde{D}_t$  is associated with the backwards Itô stochastic differential equation (SDE) on  $0 \leq s \leq T$ ,

$$\hat{d}\tilde{\mathbf{A}}_T^s(\mathbf{x}) = \mathbf{u}(\tilde{\mathbf{A}}_T^s(\mathbf{x}), s) ds + \sqrt{2\mu} \hat{d}\tilde{\mathbf{W}}(s); \quad (2a)$$

$$\tilde{\mathbf{A}}_T^T(\mathbf{x}) = \mathbf{x}. \quad (2b)$$

Here,  $\hat{d}$  denotes the backward Itô differential, and  $\tilde{\mathbf{W}}(s)$  is a vector where each component is an independent standard Wiener process (i.e. Brownian motion). The SDE (2) governs the motion of Lagrangian particles tracking the flow backward in time from a point  $\mathbf{x} \in D$  at time  $T$ , perturbed by white noise.  $\tilde{\mathbf{A}}_T^s(\mathbf{x})$  is called the ‘stochastic back-to-labels’ map in [33].

Frequently, we are interested in the integrated solutions of (1) with respect to some function  $\eta(\mathbf{x})$ . If we can write  $\eta(\mathbf{x}) = w(\mathbf{x})p(\mathbf{x})$  for some probability density  $p(\mathbf{x})$  and weight function  $w(\mathbf{x})$ , this integral can be expressed using solutions to (2) at any time  $0 \leq s \leq T$  as

$$\int_D \chi(\mathbf{x}, T) \eta(\mathbf{x}) d\mathbf{x} = \mathbb{E} \left[ \chi(\tilde{\mathbf{A}}_T^s(\mathbf{X}), s) w(\mathbf{X}) \right] + \int_s^T \mathbb{E} \left[ f(\tilde{\mathbf{A}}_T^\tau(\mathbf{X}), \tau) w(\mathbf{X}) \right] d\tau \quad (3)$$

where the expectation  $\mathbb{E}$  is taken over realizations of Brownian motion and a random variable  $\mathbf{X} \in D$  which is distributed according to the probability density  $p(\mathbf{x})$ .

We call (3) the *spectral-Lagrangian bridge*, as it gives an exact expression for spectral quantities, such as the Fourier coefficients of  $\chi$ , in terms of stochastic Lagrangian trajectories of the flow  $\mathbf{u}$ . Note that the right-hand side is linear in the solution  $\chi$  and the forcing  $f$ , reflecting the linearity of the operator  $\tilde{D}_t$ . Stochastic Lagrangian techniques can be generalized beyond the scalar problem here to include boundaries, vortex stretching in 3d, and other effects [33–36].

*Vortex reinforcement by  $\beta$ -effect.*—One Eulerian characterization of vortices is that they correspond to peaks in the vorticity field  $\zeta := \partial_x v - \partial_y u$ . Here, we consider the coarse-grained vorticity  $\zeta_\ell := g_\ell * \zeta$ , which is convolved with  $g_\ell(\mathbf{x}) := \ell^{-2} g(\mathbf{x}/\ell)$  where  $g$  is a 2d unit Gaussian. Noting that  $\int_D g \zeta d\mathbf{x} = \int_D \mathbf{w} \cdot \mathbf{u} d\mathbf{x}$  where  $\mathbf{w} := (\partial_y g, -\partial_x g)$ , the coarse-grained vorticity has a spectral interpretation in terms of the alignment of the velocity field with wavelets of the form  $\mathbf{w}_\ell$ . To compute  $\zeta_\ell$  using the spectral-Lagrangian bridge (3), we fix a mea-

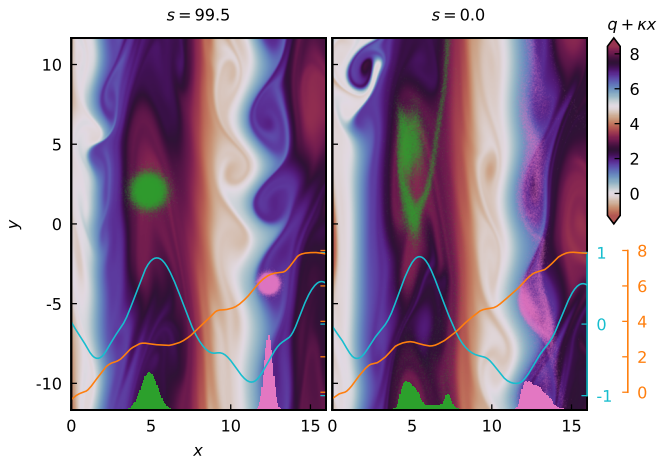


FIG. 2. Two frames showing stochastic tracers (green, pink) at different times  $s = 99.5, 0$  plotted on top of the potential vorticity field  $q + \kappa x$ . Histograms of the  $x$  positions of the tracers are plotted at the bottom of the frames, showing the resulting skewed distribution of tracers. Profiles of the instantaneous zonally-averaged zonal flow (cyan) and zonally-averaged PV (orange) are shown as well.

surement time  $T = 99.5$  and initialize a Gaussian patch of stochastic tracers at time  $s = T$  inside some of the coherent vortex structures, then evolve them backwards in time until  $s = 0$ . These tracers are shown in Fig. 2, and in a movie available in the supplementary material.

Substituting the BHW PV,  $\chi = q + \kappa x = \zeta - \tilde{n} + \kappa x$ , into (3), where  $\tilde{n}$  is the non-zonal component of the electron density, we identify four contributions to the coarse-grained vorticity  $\zeta_\ell = \zeta_{coh} + \zeta_n + \zeta_\kappa + \zeta_\Delta$ . The first three are given by

$$\zeta_{coh} = \mathbb{E} \left[ \zeta(\tilde{\mathbf{A}}_T^s(\mathbf{X}), s) w(\mathbf{X}) \right] \quad (4a)$$

$$\zeta_n = \mathbb{E} \left[ \left( \tilde{n}(\mathbf{X}, T) - \tilde{n}(\tilde{\mathbf{A}}_T^s(\mathbf{X}), s) \right) w(\mathbf{X}) \right] \quad (4b)$$

$$\zeta_\kappa = \mathbb{E} \left[ \kappa \tilde{\mathbf{x}} \cdot \left( \mathbf{X} - \tilde{\mathbf{A}}_T^s(\mathbf{X}) \right) w(\mathbf{X}) \right] \quad (4c)$$

First,  $\zeta_{coh}$  is the value of the vorticity that would arise from stirring of a passive scalar field with initial conditions  $\zeta(\mathbf{x}, s)$  at time  $s$ . Due to turbulent mixing and diffusion, we expect that  $\zeta_{coh} \rightarrow 0$  as  $(T - s) \rightarrow \infty$ , i.e. as the measurement time  $T$  gets further away from the initial time  $s$ . If the vortices did not exchange fluid with the rest of the flow, displaying Lagrangian coherence,  $\zeta_{coh}$  would decay on the diffusive timescale  $O(10^3)$  for vortices of size  $O(1)$ .

Second,  $\zeta_n$  and  $\zeta_\kappa$  are the components of vorticity that arise to match changes in the non-zonal  $\tilde{n}$  and background gradient  $\kappa x$  components of the electron density. Note that  $\zeta_\kappa$  is proportional to the average change in the  $x$  position of the tracer particles. In the geophysical case,  $\zeta_n$  and  $\zeta_\kappa$  track changes in vorticity due to vertical vortex stretching and the  $\beta$ -effect respectively.

Finally,  $\zeta_\Delta$  is the unresolved vorticity contribution due

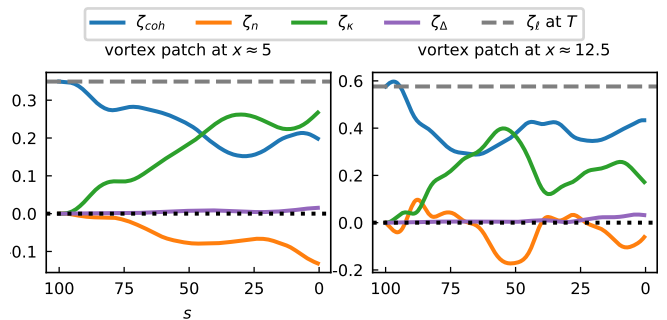


FIG. 3. Two plots showing the contributions of different terms to the coarse-grained vorticity  $\zeta_\ell$  for the two different tracer patches in Fig. 2.  $s$  evolves backwards from the measurement time  $T$ . The four solid lines in color will always add up to  $\zeta_\ell$  measured at  $T$ , shown in dashed grey.

to the hyperviscosity added for numerical stability, as well as the approximation errors introduced by the numerical methods used to solve the original PDEs and Lagrangian SDEs.

In Fig. 3, we plot these four quantities for the two patches of tracers shown in Fig. 2. Some tracers have left the initial patch, indicating that the vortex has exchanged fluid with the rest of the domain. As illustrated by  $\zeta_{coh}$ , the vortex amplitudes would have dropped by around one-third due to mixing over the time interval, necessitating some mechanism beyond Lagrangian coherence to sustain the vortex. Looking at  $\zeta_\kappa$ , we observe that the  $\beta$ -effect is primarily responsible for maintaining the observed vorticity.

Kinematically, this effect can be understood through the tendency for co-rotating vortices to entrain tracers from larger  $x$ , illustrated by the histograms plotted in Fig. 2. Similarly, counter-rotating vortices tend to entrain tracers from smaller  $x$ , maintaining them against mixing and dissipation as well. A zonally homogeneous radial mixing of tracers would not be able to produce this observed pattern of transport.

*Chaotic Tangles.*—To explain the zonally inhomogeneous transport, we first focus on the vortex patch located around  $x \approx 5$ . The distribution of tracers at  $s = 68$  is shown in Fig. 4a. Notice that the tracers exiting the vortex are drawn out into long filaments. Close to where they attach to the vortex, the tracer filaments transversally intersect filaments in the PV field.

The transversally intersecting filaments can be understood through the presence of attracting and repelling Lagrangian Coherent Structures (LCSs) in the flow, collectively referred to as hyperbolic LCSs. In planar flows, attracting (repelling) LCSs can be defined as material curves which have strong transverse attraction forward (backwards) in time [37]. By computing finite-time Lyapunov exponents (FTLEs), shown in Fig. 4b, we can heuristically detect the presence of hyperbolic LCSs [38]. Notice that PV filaments, which are advected forward in time, align with the attracting LCSs in red. Tracer

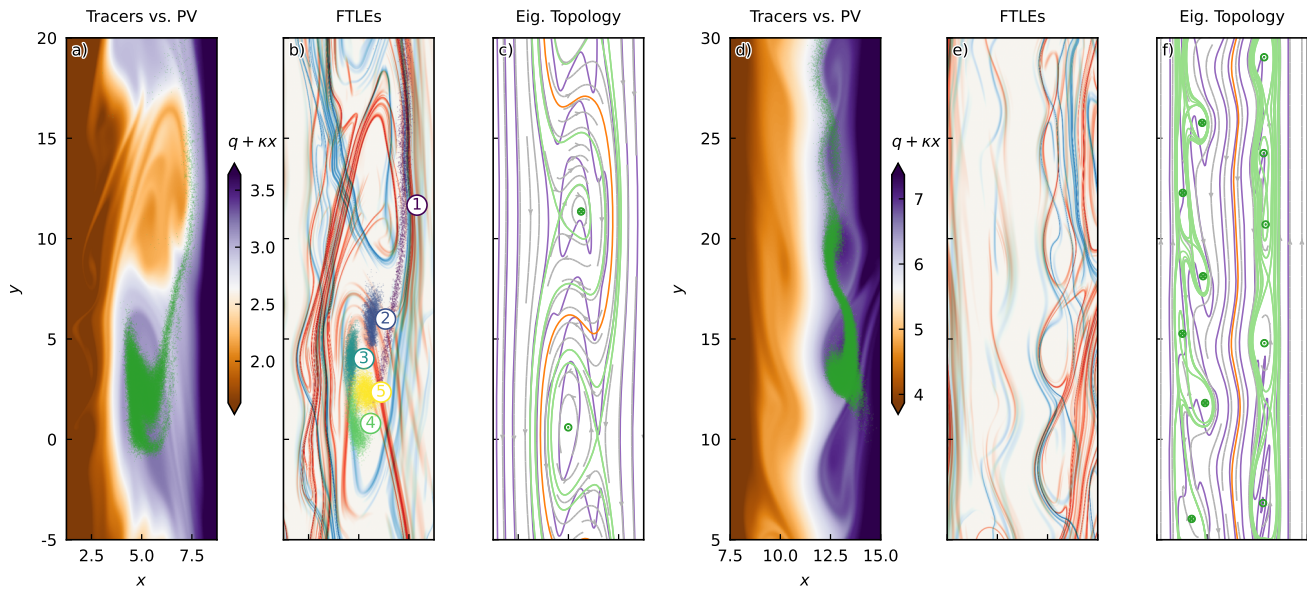


FIG. 4. (a) Tracers in green overplotted on the PV field for one band of vortices, showing transversal filamentary structures. (b) Plot of forward and backward finite-time Lyapunov exponents (FTLEs), with attracting/repelling exponents in red/blue respectively. The time history of a single tracer filament is overplotted. (c) Streamplot showing flows in the co-moving frame induced by trapped drift-Rossby wave eigenmodes. Flow topology is shown with separatrices and O-points with sense of rotation in green and the nontwist torus in orange. Level sets of the wavy PV are shown in purple. (d-f) are similarly marked plots.

filaments, advected backwards in time, align with the repelling LCSs in blue. Similar to past studies [39–42], we find transversally intersecting attracting and repelling LCSs, indicative of the chaotic tangle-like structure.

By utilizing these LCSs, we can explain how chaotic transport tends to reinforce the vortex. Fig. 4b shows the time evolution of one tracer filament over five equally spaced snapshots from  $s = 0$  at step 1 to  $s = 99.5$  at step 5. In step 1, the tracer filament transversally crosses PV filaments outside the vortex. Transport of PV into the filament is dominated by diffusion, akin to a ‘bucket’ of fluid being filled diffusively with PV.

Backwards in time from step 2  $\rightarrow$  1, tracers are stretched by their attraction to the repelling LCS. Forwards in time 1  $\rightarrow$  2 this stretching is undone. Advective transport then overtakes diffusive PV transport in steps 2  $\rightarrow$  4, akin to the ‘bucket’ being passed along by the vortical flow. Notably, in step 3  $\rightarrow$  4 the tracers pass through the vortex boundary in a manner reminiscent of lobes passing through a turnstile [43].

Finally, in step 5 the tracers are fully entrained into the vortex, emptying the ‘PV bucket’ into the vortex. The net movement of the tracers was from larger to smaller  $x$ , strengthening the vortex via the  $\beta$ -effect. Many of these filaments form during the backwards evolution of the tracer patch, akin to a ‘brigade’ of ‘PV buckets’.

Focusing now on the vortex patch around  $x \approx 12.5$ , the filament kinematics are more complicated. Comparing Fig. 4d to Fig. 4e, we can again see that tracer filaments tend to align with repelling LCSs and PV filaments align with attracting LCSs. In contrast to the earlier

case, tracers can leave the vortex through the transversal LCS intersections in either the ‘upstream’ (prograde) or ‘downstream’ (retrograde) directions. Following the repelling LCSs, the upstream tracers tend to be re-trapped into vortices, leading to no overall transport in  $x$ . Meanwhile, the downstream tracers tend to get lost in the chaotic regions at larger  $x$ . The net effect, as quantified in Fig. 3, is that the vortex is reinforced.

*Nearly-integrable Flow Topology.*—We now turn to explain how the tangled LCSs can arise from the self-consistent dynamics of the fluid. Linearizing around the zonally and temporally averaged zonal flow and density profiles results in an eigenvalue equation for modes which propagate in  $y$  but are localized in  $x$  (see the supplementary material). Plotted in Fig. 4c and f are approximations to the flow fields using the zonal flows plus 3-4 eigenmodes in each case. Streamplots are shown for the instantaneous frozen velocity field in a frame of reference co-moving with the phase velocity of the dominant eigenmode.

Comparing Fig. 4c,f with Fig. 4b,e, there is a clear resemblance between the observed hyperbolic LCSs and the eigenmode streamline topologies. Furthermore, these resemble topologies observed for Rossby waves propagating in the Bickley jet and the related standard nontwist map [44–46]. The larger vortices exhibit a homoclinic nontwist topology, and are linked to drift-Rossby waves trapped in the retrograde jets. The smaller vortices exhibit a heteroclinic nontwist topology, and are linked to waves localized near the sharp PV interface associated with the prograde jets.

Despite their resemblance to linear structures, the vortices here are large amplitude. PV perturbations from the vortices can be as large as the corrugations of the zonal PV, which in turn can be as steep as the background PV gradient. Additionally, for the large vortices the maximal vortex rotation rates  $\omega_{vortex} \approx 0.23$  are close to the maximal FTLEs  $\lambda_{lyap} \approx 0.23$ , so quasilinear theory cannot be justified here by the rapidity of the fluid parcel detrapping time relative to the eddy circulation time [47].

Linear dispersion is also not necessarily balanced against nonlinear effects, unlike the case for KdV-like drift-Rossby solitons [48]. For example, the variation in vortex sizes seen in in Fig. 4d evolves like an amplitude modulation of a  $\lambda_y = L_y/6$  carrier wave with an observed group velocity of  $v_{gr,obs} \approx -0.61$ , close to the linear group velocity of  $v_{gr,eig} \approx -0.64$  and differing from the linear phase velocity of  $v_{ph,eig} \approx -0.4$ .

To explain why the eigenmode flow topology persists, we build on the near-integrability property for drift-Rossby eigenmodes proposed in [49]. Following [21], the fact that the PV is an integral of motion in the ideal case can be viewed as a commutation condition between the Lagrangian flows and a fluid element relabeling symmetry generated by the PV. Near-integrability states that the ‘wavy’ eigenmode plus zonal background PV acts as a near-integral of motion, generating a relabeling which formally satisfies a certain optimal near-commutation condition with the wave-induced Lagrangian flows. This is illustrated in Fig. 4c,f, where the contours of the wavy PV are nearly aligned with the eigenmode streamlines.

Physically, this can be interpreted as follows: in the moving reference frame, the coherent vortex structures appear nearly stationary from an Eulerian viewpoint. Such structures are surprising from a Lagrangian viewpoint, as the stationarity results from a constantly evolving configuration of fluid elements. Near-integrability reconciles these two viewpoints by suggesting the existence of a relabeling symmetry that can approximately undo the action of the Lagrangian flows. Advected fluid elements can be relabeled to approximately resemble a stationary reference configuration, thus accounting for the observed Eulerian coherence.

The alignment of the hyperbolic LCSs with the eigenmode streamlines shows that the formal near-integrability survives in practice, suggesting that the attracting/repelling LCSs originate from separatrix splitting in the nearly-integrable flow. Furthermore the corresponding chaotic regions do not penetrate too deeply into either the jet or vortex cores, preserving the wavy PV

distribution which supports the nearly-integrable flow.

*PV Staircases.*—Finally, we observe that the vortices induce a radially inhomogeneous mixing compatible with the PV staircase paradigm. For the heteroclinic-type vortices in the prograde jets, mixing tends to occur on the flanks of the jets, further sharpening the PV jump which supports the jet. For the homoclinic-type vortices in the retrograde jets, the non-twist torus has a much stronger meander. Upon zonal averaging, this leads to the flattened PV region which supports the retrograde jets. These jets then act as a waveguide supporting localized drift-Rossby eigenmodes, closing the loop on the bucket brigade mechanism.

*Discussion.*—The physical picture here demonstrates that the turbulence is dominated by horizontal convective rolls which sufficiently relax the background driving gradients as to largely extinguish the growth of other primary instabilities. The PV bucket brigade describes the mechanism by which these rolls sustain themselves through the entrainment and subsequent radial transport of fluid into themselves. These vortical rolls look ‘approximately the same’ under flow advection, which is understood through an eigenmode near-integrability property linked to the fluid element relabeling symmetry.

Although the system studied here is highly idealized and not strongly driven, the topological structures and other key parts of the bucket brigade mechanism align with phenomenology observed in similar physical systems. The homoclinic-type vortices studied here bear resemblance to the flow topology of  $\Omega$ -type atmospheric blocks, where the role of quasi-horizontal PV advection and Rossby waves has been well-studied [17, 18, 50]. The heteroclinic-type vortices resemble structures seen in Kelvin-Helmholtz wave instabilities [51] and high Reynolds number wall-driven 2d channel flow [52]. Given the rich variety of structures exhibiting Lagrangian coherence in nature [37, 53], it would be interesting to see if the ideas based on the spectral-Lagrangian bridge and relating near-integrability with relabeling symmetries can be generalized to describe structure formation beyond the system studied here.

## ACKNOWLEDGMENTS

The authors thank P.J. Morrison and E. VandenEijnden for valuable discussions that contributed to this work. N.M.C. acknowledges support by the US DOE under grant DE-FG02-04ER54742. D.Q. acknowledges support by ONR grant N00014-24-1-2192.

- 
- [1] P. S. Marcus, Jupiter’s Great Red Spot and Other Vortices, *Annual Review of Astronomy and Astrophysics* **31**, 523 (1993).  
 [2] A. R. Vasavada and A. P. Showman, Jovian atmospheric dynamics: an update after Galileo and Cassini, *Reports*

- on *Progress in Physics* **68**, 1935 (2005).  
 [3] P. L. Read, The Dynamics of Jupiter’s and Saturn’s Weather Layers: A Synthesis After Cassini and Juno, *Annual Review of Fluid Mechanics* **56**, 271 (2024).  
 [4] V. Wirth, M. Riemer, E. K. M. Chang, and O. Martius,

- Rosby Wave Packets on the Midlatitude Waveguide—A Review, *Monthly Weather Review* **146**, 1965 (2018).
- [5] N. Nakamura and C. S. Y. Huang, Atmospheric blocking as a traffic jam in the jet stream, *Science* **361**, 42 (2018).
- [6] F. Wagner, A quarter-century of H-mode studies, *Plasma Physics and Controlled Fusion* **49**, B1 (2007).
- [7] G. Dif-Pradalier, G. Hornung, P. Ghendrih, Y. Sarazin, F. Clairet, L. Vermare, P. H. Diamond, J. Abiteboul, T. Cartier-Michaud, C. Ehrlacher, D. Estève, X. Garbet, V. Grandgirard, Ö. D. Gürcan, P. Hennequin, Y. Kosuga, G. Latu, P. Maget, P. Morel, C. Norscini, R. Sabot, and A. Storelli, Finding the Elusive ExB Staircase in Magnetized Plasmas, *Physical Review Letters* **114**, 085004 (2015).
- [8] G. Hornung, G. Dif-Pradalier, F. Clairet, Y. Sarazin, R. Sabot, P. Hennequin, and G. Verdoolaege,  $\mathbf{E} \times \mathbf{B}$  staircases and barrier permeability in magnetised plasmas, *Nuclear Fusion* **57**, 014006 (2017).
- [9] W. Liu, Y. Chen, R. Ke, G. McKee, Z. Yan, K. Fang, Z. Yang, Z. Gao, Y. Tan, and G. R. Tynan, Evidence of  $\mathbf{E} \times \mathbf{B}$  staircase in HL-2A L-mode tokamak discharges, *Physics of Plasmas* **28**, 10.1063/5.0022679 (2021).
- [10] L. Qi, M. Choi, J.-M. Kwon, and T. Hahm, Role of zonal flow staircase in electron heat avalanches in KSTAR L-mode plasmas, *Nuclear Fusion* **61**, 026010 (2021).
- [11] P. Müller, Ertel's potential vorticity theorem in physical oceanography, *Reviews of Geophysics* **33**, 67 (1995).
- [12] A. J. Thorpe and C. H. Bishop, Potential vorticity and the electrostatics analogy: Ertel—Rossby formulation, *Quarterly Journal of the Royal Meteorological Society* **121**, 1477 (1995).
- [13] N. Padhye and P. Morrison, Fluid element relabeling symmetry, *Physics Letters A* **219**, 287 (1996).
- [14] P. H. Diamond, S. I. Itoh, K. Itoh, and T. S. Hahm, Zonal flows in plasma - A review, *Plasma Physics and Controlled Fusion* **47**, R35 (2005), arXiv:1302.4625.
- [15] Y. Wang, A. Gozolchiani, Y. Ashkenazy, Y. Berezin, O. Guez, and S. Havlin, Dominant Imprint of Rossby Waves in the Climate Network, *Physical Review Letters* **111**, 138501 (2013), arXiv:1304.0946.
- [16] T. Woollings, C. Li, M. Drouard, E. Dunn-Sigouin, K. A. Elmetekawy, M. Hell, B. Hoskins, C. Mbengue, M. Patterson, and T. Spengler, The role of Rossby waves in polar weather and climate, *Weather and Climate Dynamics* **4**, 61 (2023).
- [17] A. M. Altenhoff, O. Martius, M. Croci-Maspoli, C. Schwierz, and H. C. Davies, Linkage of atmospheric blocks and synoptic-scale Rossby waves: a climatological analysis, *Tellus A: Dynamic Meteorology and Oceanography* **60**, 1053 (2008).
- [18] R. H. White, K. Kornhuber, O. Martius, and V. Wirth, From Atmospheric Waves to Heatwaves: A Waveguide Perspective for Understanding and Predicting Concurrent, Persistent, and Extreme Extratropical Weather, *Bulletin of the American Meteorological Society* **103**, E923 (2022).
- [19] D. G. Dritschel and M. E. McIntyre, Multiple Jets as PV Staircases: The Phillips Effect and the Resilience of Eddy-Transport Barriers, *Journal of the Atmospheric Sciences* **65**, 855 (2008).
- [20] Ö. D. Gürcan and P. H. Diamond, Zonal flows and pattern formation, *Journal of Physics A: Mathematical and Theoretical* **48**, 293001 (2015).
- [21] N. M. Cao and D. Qi, Nearly integrable flows and chaotic tangles in the Dimits shift regime of plasma edge turbulence, *Physics of Plasmas* **30**, 10.1063/5.0158013 (2023).
- [22] A. Dimits, B. Cohen, N. Mattor, W. Nevins, D. Shumaker, S. Parker, and C. Kim, Simulation of ion temperature gradient turbulence in tokamaks, *Nuclear Fusion* **40**, 661 (2000).
- [23] P. H. Diamond and T. S. Hahm, On the dynamics of turbulent transport near marginal stability, *Physics of Plasmas* **2**, 3640 (1995).
- [24] C. Connaughton, S. Nazarenko, and B. Quinn, Rossby and drift wave turbulence and zonal flows: The Charney–Hasegawa–Mima model and its extensions, *Physics Reports* **604**, 1 (2015).
- [25] A. Hasegawa and M. Wakatani, Plasma Edge Turbulence, *Physical Review Letters* **50**, 682 (1983).
- [26] C. J. McDevitt, P. H. Diamond, Ö. D. Gürcan, and T. S. Hahm, Poloidal rotation and its relation to the potential vorticity flux, *Physics of Plasmas* **17**, 112509 (2010).
- [27] J. Madsen, J. J. Rasmussen, V. Naulin, A. H. Nielsen, and F. Treue, Gyrofluid potential vorticity equation and turbulent equipartition states, *Plasma Physics and Controlled Fusion* **57**, 054016 (2015).
- [28] A. J. Majda, D. Qi, and A. J. Cerfon, A flux-balanced fluid model for collisional plasma edge turbulence: Model derivation and basic physical features, *Physics of Plasmas* **25**, 102307 (2018).
- [29] D. Qi, A. J. Majda, and A. J. Cerfon, A flux-balanced fluid model for collisional plasma edge turbulence: Numerical simulations with different aspect ratios, *Physics of Plasmas* **26**, 10.1063/1.5083845 (2019), arXiv:1812.00131.
- [30] D. Qi and A. J. Majda, Flux-balanced two-field plasma edge turbulence in a channel geometry, *Physics of Plasmas* **27**, 032304 (2020).
- [31] D. Qi, A. J. Majda, and A. J. Cerfon, Dimits shift, avalanche-like bursts, and solitary propagating structures in the two-field flux-balanced Hasegawa–Wakatani model for plasma edge turbulence, *Physics of Plasmas* **27**, 102304 (2020), arXiv:2006.10554.
- [32] P. Constantin and G. Iyer, A stochastic Lagrangian representation of the three-dimensional incompressible Navier-Stokes equations, *Communications on Pure and Applied Mathematics* **61**, 330 (2008).
- [33] G. L. Eyink, A. Gupta, and T. A. Zaki, Stochastic Lagrangian dynamics of vorticity. Part 1. General theory for viscous, incompressible fluids, *Journal of Fluid Mechanics* **901**, A2 (2020).
- [34] G. L. Eyink, Stochastic line motion and stochastic flux conservation for nonideal hydromagnetic models, *Journal of Mathematical Physics* **50**, 10.1063/1.3193681 (2009).
- [35] D. D. Holm, Variational principles for stochastic fluid dynamics, *Proceedings of the Royal Society A: Mathematical, Physical and Engineering Sciences* **471**, 20140963 (2015), arXiv:1410.8311.
- [36] N. Besse, Stochastic Lagrangian perturbation of Lie transport and applications to fluids, *Nonlinear Analysis* **232**, 113249 (2023).
- [37] G. Haller, Lagrangian Coherent Structures, *Annual Review of Fluid Mechanics* **47**, 137 (2015).
- [38] G. Haller, Lagrangian coherent structures from approximate velocity data, *Physics of Fluids* **14**, 1851 (2002).
- [39] N. Malhotra and S. Wiggins, Geometric Structures, Lobe

- Dynamics, and Lagrangian Transport in Flows with Aperiodic Time-Dependence, with Applications to Rossby Wave Flow, *Journal of Nonlinear Science* **8**, 401 (1998).
- [40] A. M. Rogerson, P. D. Miller, L. J. Pratt, and C. K. R. T. Jones, Lagrangian Motion and Fluid Exchange in a Barotropic Meandering Jet\*, *Journal of Physical Oceanography* **29**, 2635 (1999).
- [41] F. J. Beron-Vera, M. J. Olascoaga, M. G. Brown, H. Koçak, and I. I. Rypina, Invariant-tori-like Lagrangian coherent structures in geophysical flows, *Chaos: An Interdisciplinary Journal of Nonlinear Science* **20**, 017514 (2010).
- [42] G. Haller and F. J. Beron-Vera, Geodesic theory of transport barriers in two-dimensional flows, *Physica D: Nonlinear Phenomena* **241**, 1680 (2012).
- [43] J. D. Meiss, Thirty years of turnstiles and transport, *Chaos: An Interdisciplinary Journal of Nonlinear Science* **25**, 097602 (2015), arXiv:1501.04364.
- [44] D. Del-Castillo-Negrete and P. J. Morrison, Chaotic transport by Rossby waves in shear flow, *Physics of Fluids A: Fluid Dynamics* **5**, 948 (1993).
- [45] D. Del-Castillo-Negrete, J. Greene, and P. Morrison, Area preserving nontwist maps: periodic orbits and transition to chaos, *Physica D: Nonlinear Phenomena* **91**, 1 (1996).
- [46] D. Del-Castillo-Negrete, Chaotic transport in zonal flows in analogous geophysical and plasma systems, *Physics of Plasmas* **7**, 1702 (2000).
- [47] P. H. Diamond, S.-I. Itoh, and K. Itoh, *Modern Plasma Physics* (Cambridge University Press, Cambridge, 2010).
- [48] L. G. Redekopp, On the theory of solitary Rossby waves, *Journal of Fluid Mechanics* **82**, 725 (1977).
- [49] N. M. Cao, Rossby waves past the breaking point in zonally dominated turbulence, *Journal of Fluid Mechanics* **958**, A28 (2023).
- [50] S. Pfahl, C. Schwierz, M. Croci-Maspoli, C. M. Grams, and H. Wernli, Importance of latent heat release in ascending air streams for atmospheric blocking, *Nature Geoscience* **8**, 610 (2015).
- [51] W. Smyth and J. Moum, Ocean Mixing by Kelvin-Helmholtz Instability, *Oceanography* **25**, 140 (2012).
- [52] G. Falkovich and N. Vladimirova, Turbulence Appearance and Nonappearance in Thin Fluid Layers, *Physical Review Letters* **121**, 164501 (2018), arXiv:1711.04580.
- [53] E. L. Rempel, A. C. Chian, S. de S. A. Silva, V. Fedun, G. Verth, R. A. Miranda, and M. Gošić, Lagrangian coherent structures in space plasmas, *Reviews of Modern Plasma Physics* **7**, 32 (2023).

## Appendix A: Supplementary Material

For a function  $f(x, y)$ , we decompose it into its zonal mean  $\bar{f}$  and fluctuation  $\tilde{f}$  as  $f = \bar{f} + \tilde{f}$  with

$$\bar{f}(x) = \frac{1}{L_y} \int_0^{L_y} f(x, y) dy.$$

The flux-balanced Hasegawa-Wakatani equations can be expressed in terms of the electrostatic potential  $\varphi(x, y, t)$ , particle density anomaly  $n(x, y, t)$ , and potential vorticity anomaly  $q(x, y, t)$  as

$$[\partial_t + \mathbf{u} \cdot \nabla] q - \kappa \partial_y \varphi = \mu \nabla^2 q, \quad (\text{A1a})$$

$$[\partial_t + \mathbf{u} \cdot \nabla] n + \kappa \partial_y \varphi = \alpha (\tilde{\varphi} - \tilde{n}) \mu \nabla^2 n, \quad (\text{A1b})$$

$$q = \nabla^2 \varphi - \tilde{n}. \quad (\text{A1c})$$

Above,  $\mathbf{u} = (-\partial_y \varphi, \partial_x \varphi)$  is the  $E \times B$  velocity.  $\alpha$  is the adiabaticity parameter, which is inversely proportional to the resistivity.  $\kappa$  is related to the background density gradient, where  $n - \kappa x$  is the total particle density. Note that the modified Hasegawa-Wakatani equations differs in the last equation, with  $q_{\text{MHW}} = \nabla^2 \varphi - n$ . Furthermore, note that the PV equation (A1a) can be rewritten as  $\tilde{D}_t[q + \kappa x] = 0$ .

Taking a background zonal flow profile  $U(x)$  and splitting the fields into zonal and fluctuating components  $q = \bar{q}(x) + \hat{q}(x)e^{i(k_y y - \omega t)}$ ,  $n = \bar{n}(x) + \hat{n}(x)e^{i(k_y y - \omega t)}$ , equations for the eigenvalues and eigenfunctions can be derived:

$$\omega \hat{q}(x) = k_y U(x) \hat{q}(x) - k_y (\bar{q}'(x) + \kappa) \hat{\varphi}(x) + i\mu (\partial_x^2 - k_y^2) \hat{q}(x), \quad (\text{A2a})$$

$$\omega \hat{n}(x) = k_y U(x) \hat{n}(x) - k_y (\bar{n}'(x) - \kappa) \hat{\varphi}(x) + i\alpha (\hat{\varphi}(x) - \hat{n}(x)) + i\mu (\partial_x^2 - k_y^2) \hat{n}(x), \quad (\text{A2b})$$

$$\hat{\varphi}(x) = (\partial_x^2 - k_y^2)^{-1} [\hat{q}(x) + \hat{n}(x)]. \quad (\text{A2c})$$

The PDEs (A1) are solved using a pseudo-spectral method with a 4th-order Runge-Kutta scheme for the time integration. The SDEs for the Feynman-Kac formula are solved using a 4th-order Runge-Kutta scheme for the deterministic part, and a Maruyama scheme for the stochastic part. The velocity field and various terms in the expectation for the spectral-Lagrangian bridge are interpolated using 3rd-order Hermite polynomial interpolation in space and linear interpolation in time. The expectation over terminal conditions and realizations of the Brownian noise is approximated by Monte Carlo sampling. The eigenfunction equations (A2) are discretized using a spectral method.